



Spectroscopic view on the interaction between the psoralen derivative amotosalen and DNA

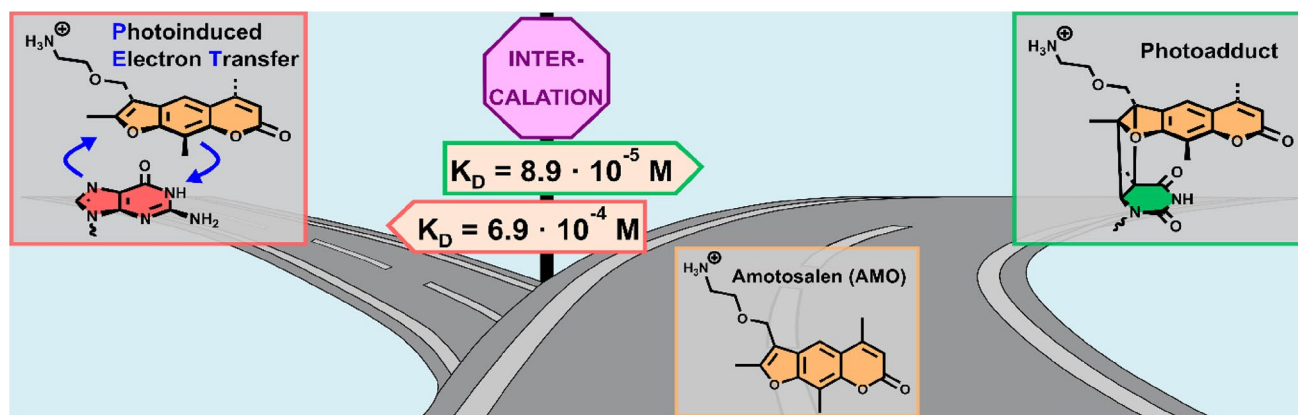
Michelle P. Rademacher¹ · Tim Rohn¹ · Wiebke Haselbach¹ · A. Theresa Ott¹ · Peter W. Bringmann² · Peter Gilch¹

Received: 15 December 2023 / Accepted: 1 February 2024 / Published online: 8 March 2024
© The Author(s) 2024

Abstract

Psoralens are eponymous for PUVA (psoralen plus UV-A radiation) therapy, which inter alia can be used to treat various skin diseases. Based on the same underlying mechanism of action, the synthetic psoralen amotosalen (AMO) is utilized in the pathogen reduction technology of the INTERCEPT[®] Blood System to inactivate pathogens in plasma and platelet components. The photophysical behavior of AMO in the absence of DNA is remarkably similar to that of the recently studied psoralen 4'-aminomethyl-4,5',8-trimethylpsoralen (AMT). By means of steady-state and time-resolved spectroscopy, intercalation and photochemistry of AMO and synthetic DNA were studied. AMO intercalates with a higher affinity into A,T-only DNA ($K_D = 8.9 \times 10^{-5}$ M) than into G,C-only DNA ($K_D = 6.9 \times 10^{-4}$ M). AMO covalently photobinds to A,T-only DNA with a reaction quantum yield of $\Phi_R = 0.11$. Like AMT, it does not photoreact following intercalation into G,C-only DNA. Femto- and nanosecond transient absorption spectroscopy reveals the characteristic pattern of photobinding to A,T-only DNA. For AMO and G,C-only DNA, signatures of a photoinduced electron transfer are recorded.

Graphical abstract



Keywords Time-resolved spectroscopy · Pathogen reduction technology · Amotosalen · DNA intercalation · Photoaddition · Photoinduced electron transfer

✉ Peter Gilch
gilch@hhu.de

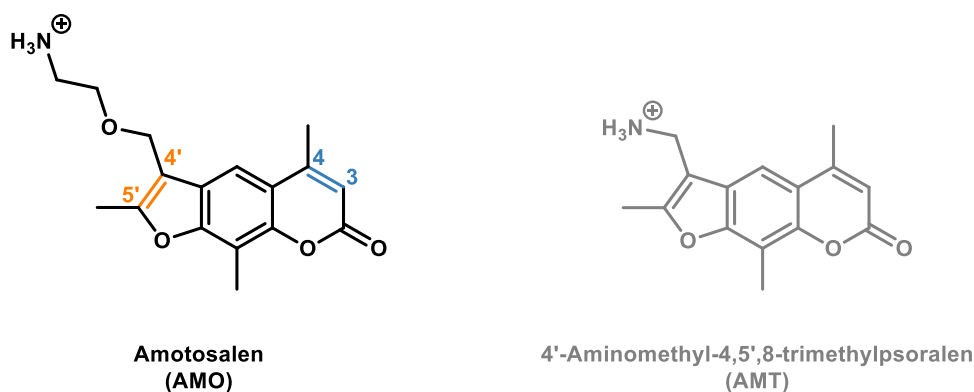
¹ Institut für Physikalische Chemie, Heinrich-Heine-Universität Düsseldorf, Universitätsstr. 1, 40225 Düsseldorf, Germany

² Cerus Corporation, 1220 Concord Avenue, Concord, CA 94520, USA

1 Introduction

Furocoumarins, particularly psoralens, occur naturally in the leaves, roots, and fruits of various plant species [1]. They have a rich history of use, spanning centuries, in traditional medicine in India, Egypt, and other oriental countries, primarily for the treatment of depigmented skin conditions,

Scheme 1. Structure of amotosalen (AMO, left) and 4'-aminomethyl-4,5',8-trimethylpsoralen (AMT, right). Potentially photoreactive double bonds of AMO are highlighted in orange (furan side) and blue (pyrone side)



such as vitiligo [2, 3]. Since the mid-1900s, psoralens have found clinical application in PUVA (psoralen plus UV-A radiation) therapy [4], which emerged as a potent treatment for an array of dermatological disorders, encompassing psoriasis [5], atopic dermatitis (neurodermatitis) [6], vitiligo [7], and cutaneous T-cell lymphoma [8]. In the field of molecular biology, synthetic psoralens were established as molecular probes to unravel RNA structure-function relationships [9–11], a methodology that was recently refined by introducing psoralen analysis of RNA interactions and structures (PARIS) [12] and its advanced iteration, PARIS2 [13]. This emphasized amotosalen's (AMO), a psoralen derivative, beneficial biochemical properties to investigate transcriptome-wide RNA base-pair interactions in living cells. Akin to PUVA therapy, the combination of AMO and UV-A light was developed to reduce pathogens in potentially contaminated blood products like platelets and plasma [14]. Moreover, AMO has recently been the focus of biochemical research characterizing plasma of convalescent COVID-19 patients [15] and investigating bacterial export mechanisms [16].

Mitigating the potential risk of contamination of blood products by pathogens of various classes, e.g., bacteria, viruses, and parasites, several technologies have been developed with the overarching goal of eliminating all pathogens while maintaining the functional integrity of the blood component. Historically, cell-free blood components, such as human plasma, underwent pathogen reduction within large plasma pools through the action of solvent/detergent (S/D) materials or by the addition of methylene blue in single plasma products within smaller blood pools [17, 18]. However, these two approaches have demonstrated limited efficacy in combatting a broad spectrum of pathogens. The S/D treatment primarily targets lipid-enveloped viruses [17], while methylene blue proves to be ineffective against certain intracellular viruses due to its inhibited permeability through the plasma membrane [18]. Furthermore, their extension to the decontamination of cell-containing blood components is impractical, as it results in substantial damage to platelets and erythrocytes. Consequently, improved

pathogen reduction technologies (PRT) have been established [19], including the MIRASOL[®] Pathogen Reduction Technology System (comprising riboflavin and broadband UV exposure from 280 to 400 nm) [20], the THERAFLEX[®] UV Platelets System (without a photosensitizing agent and exclusively narrowband UV-C light at 254 nm) [21], and the INTERCEPT[®] Blood System (combining amotosalen and UV-A exposure ranging from 320 to 400 nm) [14]. As the photophysics of AMO (Scheme 1, left) is the topic of this study, a few details on INTERCEPT[®] will be given here.

The INTERCEPT[®] Blood System, categorized as a Class III medical device, has gained its CE mark for platelets in 2002 as well as for plasma in 2006 [14], and was approved in 2014 by the Food and Drug Administration (FDA) for both blood components. Its practice extends across more than 30 countries [22]. The PRT consisting of the aforementioned AMO and UV-A irradiation has demonstrated broad efficacy for inactivating numerous enveloped as well as non-enveloped viruses and protozoan parasites [23], as well as bacteria (Gram-negative, Gram-positive, spirochetes) [24], and leukocytes [25]. However, the inactivation of some non-enveloped viruses (e.g., human parvovirus B19) [26] is limited and bacterial spores (*Bacillus cereus*) [14] are not impacted at all. These entities, while less prevalent than more sensitive pathogens transmitted via blood components, may elude the comprehensive reach of the INTERCEPT[®] Blood System for platelets and plasma. In addition, the application of the AMO/UV-A technology in erythrocyte concentrates is not practical due to the strong absorption of UV-A light by hemoglobin.

The underlying molecular mechanisms of AMO's photobiological activity (and other psoralens) involve two successive steps: in the absence of illumination, psoralens permeate cellular and nuclear membranes, intercalating between helical DNA (or RNA) base pairs. Upon subsequent photoexcitation, irreversible nominal [2 + 2] cycloadditions between the intercalated compound and adjacent thymine (or uracil) bases may occur. Thereby, covalent bonds can be formed either at the furan side via the C₄=C₅ double bond or at the pyrone side involving the C₃=C₄ of the psoralen

(see Scheme 1) [4, 27]. Furan monoadducts were shown to be capable of absorbing an additional UV-A photon and to bind to a second thymine (or uracil) base via the pyrone side, resulting in the formation of interstrand cross-links (ICL). Both monoadducts and cross-links may inhibit DNA replication and cellular proliferation [28].

AMO is closely related to 4'-aminomethyl-4,5',8-trimethylpsoralen (AMT, Scheme 1, right), which was used by our group as a model system to study the molecular mechanisms underlying the PUVA process [29–31]. By means of time-resolved spectroscopy, we revealed a photoinduced electron transfer (PET) [29, 30] competing with the photoaddition as well as the mechanism of the photoaddition [31]. In the PET process, the photoexcited psoralen is quenched by reductive electron transfer whereby the base guanine acts as donor. Studies with synthetic, guanine-free DNA (A,T-only DNA; see Sect. 2) showed that the photoaddition occurs on the microsecond time scale. It proceeds via the local triplet state of the psoralen as well as a triplet biradical in which the psoralen is bound to the thymine base via a covalent bond [31].

Here, it is scrutinized whether and to which extent the spectroscopic findings characterizing the AMT-DNA interaction can be transferred to AMO-DNA. Our spectroscopic experiments show that AMT and AMO behave very similarly in terms of photoinduced processes. However, unlike AMT, AMO exhibits a significantly higher affinity for A,T-only DNA than for G,C-only DNA.

2 Experimental section

2.1 Samples and general conditions

Amotosalen hydrochloride was purchased from MedChem-Express (> 98%). Coumarin 120 was supplied by Radiant Laser Dyes. Pure water (Fisher Chemical, HPLC gradient grade) and methanol (VWR Chemicals, HPLC gradient grade, $\geq 99.8\%$) were used as solvents. The HPLC-purified and lyophilized DNA oligomers were purchased from Sigma-Aldrich. A,T-only (5'-(TA)₂₀-3') single strands were employed to form double strands consisting of 40 base pairs. G,C-only (5'-(GC)₄-3') single strands were employed to form double strands consisting of 8 base pairs. Longer A,T-strands were employed because of the lower propensity of A,T-only DNA to form double strands [32]. Solutions of the oligonucleotides were buffered with PBS (Sigma-Aldrich, one tablet dissolved in 200 mL yielded 10 mM phosphate

buffer, 2.7 mM potassium chloride, 137 mM sodium chloride, pH 7.4 at 25 °C). Annealing of the oligonucleotide strands in solution was performed 24 h before the measurements. The solution was heated in a water bath up to 95 °C and cooled down to room temperature within several hours. All DNA concentrations refer to base pairs (bp). This is required due to the different strand lengths of A,T-only and G,C-only DNA.

2.2 Steady-state spectroscopy

The UV/Vis absorption spectra were recorded with a two-beam spectrometer from PerkinElmer (Lambda 19). Fused silica cuvettes with path lengths of 0.1 cm or 1 cm from Hellma were employed due to different sample concentrations. The fluorescence spectra were recorded in right-angle detection (FluoroMax-4, Horiba Scientific). The absorption at the excitation wavelength was ≤ 0.05 at a path length of 1 cm to avoid inner filter effects. The spectra were corrected for the spectral sensitivity of the instrument. Coumarin 120 in methanol ($\Phi_{\text{fl}}=0.51$ [33]) was employed as a reference for the determination of fluorescence quantum yields.

The intercalation affinity is quantified using the dissociation constant K_D (cf. Eq. (1)):

$$K_D = \frac{[\text{AMO}] \cdot [\text{DNA}]}{[\text{AMO}]_{\text{int}}} = \frac{[\text{AMO}] \cdot ([\text{DNA}]_0 - [\text{AMO}]_{\text{int}})}{[\text{AMO}]_{\text{int}}} \quad (1)$$

Here, $[\text{AMO}]_{\text{int}}$ is the concentration of intercalated AMO, $[\text{AMO}]$ the concentration of free AMO, $[\text{DNA}]_0$ the total concentration of DNA base pairs and $[\text{DNA}]$ the concentration of free DNA base pairs (not subject to intercalation). A small K_D indicates a high intercalation affinity. Due to the hypochromic effect caused by the intercalation of psoralens into DNA, the absorption of the mixture at the detection wavelength, A_{mix} , is lower than the one of free AMO, A_{free} . K_D values were determined spectroscopically from titration experiments [30, 34]. There, the total concentration of AMO ($[\text{AMO}] + [\text{AMO}]_{\text{int}}$) is kept constant while $[\text{DNA}]_0$ is gradually decreased. A detailed description of the protocol can be found in Ref. [30].

The impact of the photoaddition on the steady-state spectra was studied by illuminating the sample solution with an LED emitting at 375 nm (NSPU510CS, Nichia). The solutions were illuminated in 1 cm cuvettes with magnetic stirring. The light power P incident on the sample was 3.75 mW. Photon equivalents (PE) were computed based

on the power P (respectively, the photon flux F_0 through the sample in mol/s) and the illumination time t_{ill} via Eq. (2):

$$\text{PE}(t_{\text{ill}}) = \frac{n_{\text{abs}}}{n_{\text{AMO}}} = \frac{F_0 \cdot \int_0^{t_{\text{ill}}} (1 - 10^{-A_{\text{exc}}(t)}) dt_{\text{ill}}}{n_{\text{AMO}}} = \frac{P \cdot \int_0^{t_{\text{ill}}} (1 - 10^{-A_{\text{exc}}(t)}) dt_{\text{ill}}}{h \cdot \frac{c}{\lambda_{\text{exc}}} \cdot N_A \cdot n_{\text{AMO}}}. \quad (2)$$

Here, n_{abs} refers to the number of absorbed photons and n_{AMO} is the number of AMO molecules in the cuvette volume. $A_{\text{exc}}(t)$ is defined as the absorption of the sample at the excitation wavelength λ_{exc} . h is the Planck constant, c the speed of light, and N_A the Avogadro number. A PE value of one implies that, on average, each psoralen molecule has absorbed one photon. The reciprocal of the calculated photon equivalents at exhaustive exposure should be approximately equal to the reaction quantum yield Φ_R . This yield was determined based on the assumption that the photoproduct does not absorb at the excitation wavelength. Under these circumstances, the concentration of the reactant $c(t_{\text{ill}})$ as a function of illumination time t_{ill} is given by Eq. (3):

$$c(t_{\text{ill}}) = \frac{\ln\left(1 - 10^{-\frac{F_0 \cdot \Phi_R}{V} \cdot \epsilon_{\text{exc}} \cdot d \cdot t_{\text{ill}}} + 10^{-\frac{F_0 \cdot \Phi_R}{V} \cdot \epsilon_{\text{exc}} \cdot d \cdot [\text{AMO}]_{\text{int}}}\right)}{\epsilon_{\text{exc}} \cdot d \cdot \ln 10}. \quad (3)$$

Here, ϵ_{exc} is the absorption coefficient of the reactant (AMO_{int}) at the excitation wavelength, V is the sample volume, $d = 1$ cm the optical pathlength and $[\text{AMO}]_{\text{int}}$ the initial concentration of AMO_{int} in the sample solution. The time-dependent concentration $c(t_{\text{ill}})$ was derived from the measured absorption as a function of illumination time $A(t_{\text{ill}})$, using Beer's law. The reaction quantum yield Φ_R was determined by fitting the experimental values using Eq. (3) as a trial function. The result was cross-checked with a linearized version of Eq. (3) applied to short illumination times.

2.3 Femtosecond transient absorption spectroscopy

The femtosecond transient absorption (fsTA) setup has been described elsewhere in more detail [35–37]. Here, only a brief description and the relevant experimental parameters are summarized. A 1 kHz Ti:Sa laser amplifier system (Coherent Libra) served as pulse source. The output has a wavelength of 800 nm and a pulse duration (full width half maximum (FWHM)) of 100 fs. A portion of its output was converted by a noncollinear OPA (TOPAS-white, Light Conversion) to 660 nm and then frequency doubled in a β -barium borate crystal to yield the pump wavelength of 330 nm. The pump pulse energy was adjusted to ~ 1 μJ and the pump beam had a focal diameter of 160 μm (FWHM) at the sample location. The absorption change was probed with

a white light continuum generated in CaF_2 with a diameter of 100 μm at the sample location. The relative polarization

of the pump and probe beam was set to the magic angle. The time resolution was ~ 180 fs. The spectra were recorded at 139 delay times. Between -1 ps and 1 ps, they were evenly spread on a linear and from 1 ps to ~ 3.3 ns on a logarithmic scale. For every delay time, 2000 spectra were recorded and the data were averaged over 4 succeeding delay line scans. The instrumental time-zero shift was determined via the optical Kerr effect as a function of wavelength and was corrected for. Signals of the pure solvent were recorded in separate measurements and subtracted after proper scaling to remove time-zero artifacts [38]. The solution was circulated through a fused silica flow cell (custom made, Hellma Analytics) with 1 mm path length. The sample volume was large enough to render contributions of photoproduct formed during an experiment negligible.

For each data set, 4 fsTA measurements were performed consecutively on one day: one on AMO in water, one on pure water, one on the AMO/DNA solution, and one on a pure DNA solution. The pure DNA sample showed no significant transient absorption signal under the chosen excitation conditions and can, therefore, be treated as the “solvent” in the correction procedure for the AMO/DNA solution. As described in a previous study [29], a scaling factor is required to remove the contribution of free AMO molecules from the AMO/DNA signals. To make the signal strengths directly comparable, the solvent-corrected data sets with $(\Delta A(\lambda, t)_{\text{meas}}^{\text{mix}})$ and without DNA $(\Delta A(\lambda, t)_{\text{meas}}^{\text{free}})$ first have to be normalized to the number of excitation photons they absorbed (cf. Eq. (4)):

$$\Delta A(\lambda, t)_{\text{corr}}^{\text{int}} = \Delta A(\lambda, t)_{\text{meas}}^{\text{mix}} - \Delta A(\lambda, t)_{\text{meas}}^{\text{free}} \cdot \frac{1 - 10^{-A_{\text{mix}}}}{1 - 10^{-A_{\text{free}}}} \cdot \frac{\epsilon_{\text{free}} \cdot [\text{AMO}]}{\epsilon_{\text{int}} \cdot [\text{AMO}]_{\text{int}} + \epsilon_{\text{free}} \cdot [\text{AMO}]}. \quad (4)$$

This is achieved by multiplying the data set without DNA with $(1 - 10^{-A_{\text{mix}}}) / (1 - 10^{-A_{\text{free}}})$. To determine the fraction of excited, free AMO molecules relative to all excited ones, the concentrations $[\text{AMO}]$ and $[\text{AMO}]_{\text{int}}$ (as deduced from the dissociation constant K_D) and absorption coefficients $\epsilon_{\text{free/int}}$ of free and intercalated AMO molecules in the mixture have to be considered. The scaling factor for the subtraction of the data set without DNA from the one with DNA is $(\epsilon_{\text{free}}[\text{AMO}] / (\epsilon_{\text{int}}[\text{AMO}]_{\text{int}} + \epsilon_{\text{free}}[\text{AMO}]$).

2.4 Nanosecond transient absorption spectroscopy

The nanosecond transient absorption (nsTA) data were acquired with a laser flash photolysis spectrometer LP980 from Edinburgh Instruments in a right-angle geometry as described in other studies [37, 39]. The third harmonic of the output wavelength (355 nm) of a Nd:YAG laser (Spitlight 600, fundamental of 1064 nm, InnoLas) with a repetition rate of 5 Hz and a pulse duration of 12 ns (FWHM) was utilized for photoexcitation. The diameter of the pump beam was ~8 mm. The average pulse energy amounted to ~2 mJ. A pulsed xenon lamp (Osram XBO 150W/CR OFR) generated the probe beam. The transmitted probe light was detected by a photomultiplier (Hamamatsu, PMT-900) after being dispersed by a grating monochromator. The signal was digitized by an oscilloscope (MDO3022, Tektronix). To obtain transient spectra, kinetic traces at different probe wavelengths were recorded and averaged over 120 acquisitions for AMO in absence of DNA and 16 acquisitions for AMO intercalated into A,T-only DNA. The solution was pumped through a fused silica flow cell (Hellma Analytics) with a path length of 2 mm in pump and 10 mm in probe direction. Due to the shorter lifetimes of AMO in water compared to AMO intercalated into A,T-only DNA, a subtraction process for the amount of free psoralen was not necessary. The measurements were performed with aerated solutions unless specified otherwise. Changes in lifetime as a function of oxygen concentration were determined at a wavelength of 360 nm. Here, sample solutions with the same concentration were either aerated, saturated with oxygen (99.999%, Air Liquide) or deoxygenated with nitrogen (99.999%, Air Liquide) (see SI, Fig. S2).

2.5 Time-correlated single-photon counting

Time-correlated single-photon counting (TCSPC) was performed on a FluoTime 300 from PicoQuant. A supercontinuum picosecond laser (SuperK Extreme equipped with SuperK Extend-UV, NKT Photonics) tuned to 350 nm served as excitation source. Emission was detected at 474 nm under magic angle conditions. The repetition rate was set to 19.5 MHz. Sample solutions with an absorption at the excitation wavelength below 0.1 were measured until a peak value of 10,000 counts was achieved. The instrumental response function (IRF) was measured with scattered light of colloidal silica gel (Ludox HS-30, Sigma-Aldrich).

2.6 Data analysis

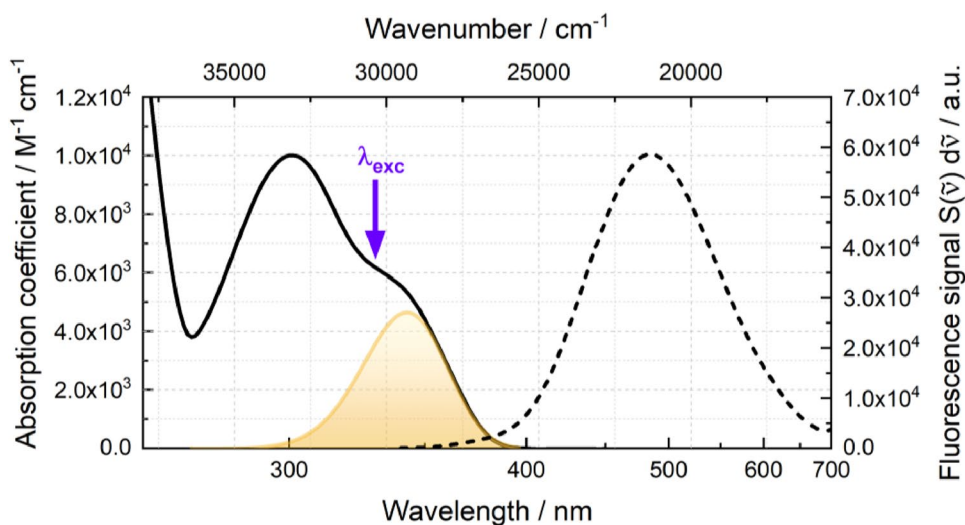
Wavelength-dependent time-resolved data were analyzed globally using a multi-exponential trial function convoluted with the IRF (cf. Eq. (5)):

$$\Delta A(\lambda, t) = \text{IRF} \otimes \sum_{i=1}^n \Delta A_i(\lambda) \cdot e^{-\frac{t}{\tau_i}}. \quad (5)$$

The fit yields a decay-associated difference spectrum (DADS) $\Delta A_i(\lambda)$ for each time constant τ_i . TCSPC data sets were fitted with a multi-exponential trial function convoluted with the IRF (cf. Eq. (6)):

$$S(t) = \text{IRF} \otimes \sum_{i=1}^n A_i \cdot e^{-\frac{t}{\tau_i}}. \quad (6)$$

Fig. 1 Comparison of the absorption coefficient spectrum (black, solid) and fluorescence emission spectrum (black, dashed) of AMO in water. The yellow line represents the absorption band lowest in energy derived from a Gaussian fit. In the fluorescence experiment, the excitation wavelength was tuned to 330 nm (arrow). The fluorescence spectrum was multiplied by wavelength squared to arrive at a representation with constant wavenumber bandpass



3 Results

3.1 Steady-state characteristics of AMO in absence of DNA

The absorption spectrum of AMO dissolved in water features an absorption band lowest in energy around 300 nm, accompanied by a shoulder around 330 nm (molar absorption coefficient $\epsilon_{330\text{nm}} = 6.6 \times 10^4 \text{ M}^{-1} \text{ cm}^{-1}$, Fig. 1). The spectrum strongly resembles the one of AMT and other psoralens [27, 28]. Quantum chemical computations on the psoralen parent compound assign the shoulder to the $S_0 \rightarrow S_1$ transition and the peak to the $S_0 \rightarrow S_2$ transition [40]. Both transitions have $\pi\pi^*$ character [40]. To isolate the lowest transition, a Gaussian fit was conducted on the absorption signals as a function of wavenumber (cf. Fig. 1).

Upon excitation of an AMO solution at 330 nm, a fluorescence spectrum peaking at 474 nm (Fig. 1) is recorded. The 0–0 excitation energy E_{00} can be derived from the intersection of the absorption and fluorescence spectra after proper plotting. For this purpose, the spectra were first transferred to an energy axis and corrected for intrinsic frequency dependencies (transition dipole representation) [41]. This yields a 0–0 excitation energy E_{00} of 3.15 eV for AMO. To quantify the efficiency of fluorescence emission, the fluorescence quantum yield Φ_{fl} was determined (see Sect. 2). It amounts to $\Phi_{\text{fl}} = 0.083$, indicating a slightly higher value compared to AMT ($\Phi_{\text{fl}} = 0.054$). Via a Strickler-Berg analysis [41, 42], the radiative rate constant k_{r}^{SB} was determined to be $2.7 \times 10^7 \text{ s}^{-1}$. Here, the shoulder in the absorption spectrum isolated by a Gaussian fit entered the evaluation (cf.

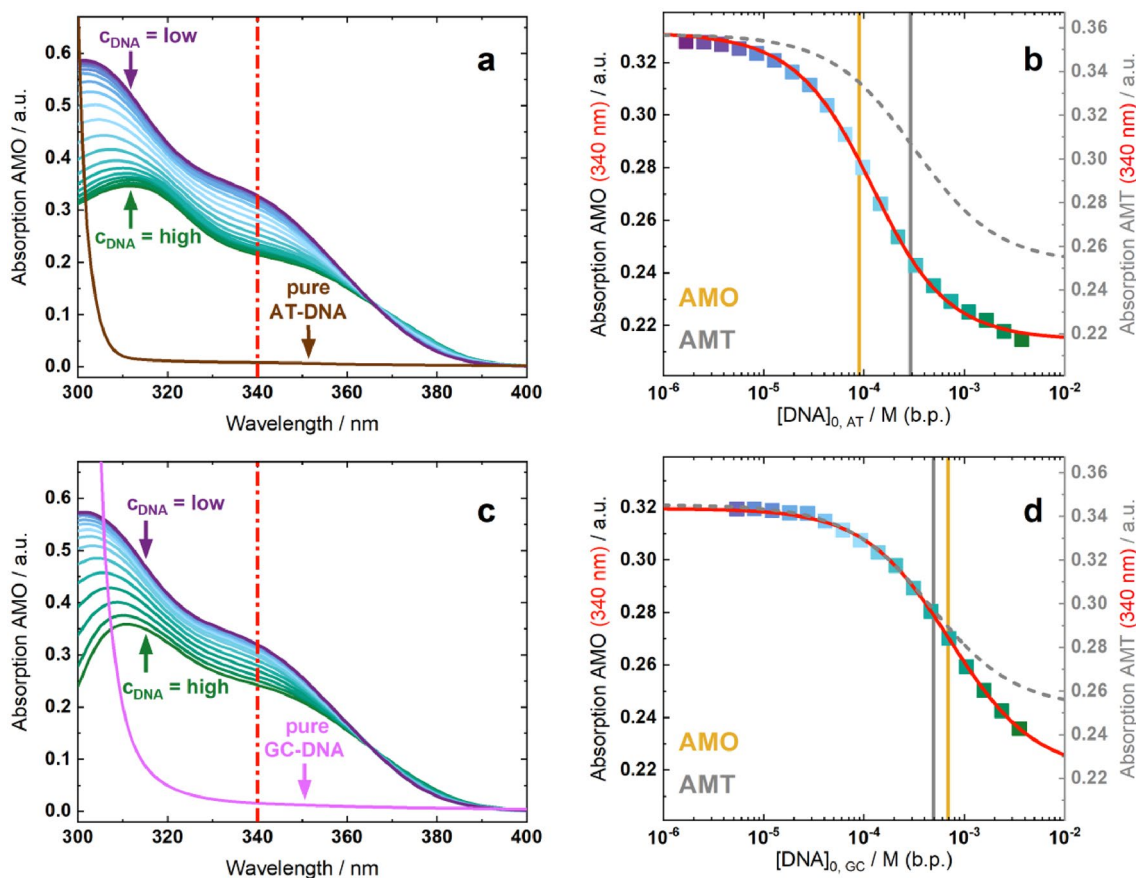


Fig. 2 Intercalation behavior of AMO into A,T-only DNA and G,C-only DNA. **(a)** UV/Vis absorption spectra of AMO (60 μM) with increasing concentration of A,T-only DNA (violet to green) in phosphate-buffered saline (PBS). The contribution of DNA to the absorption was subtracted. The spectrum of pure A,T-only DNA (4 mM) is shown in brown. **(b)** Absorption at 340 nm versus the concentration of A,T-only DNA $[\text{DNA}]_{0, \text{AT}}$. A fit (red) yields the dissociation constant $K_{\text{D}} = 8.9 \times 10^{-5} \text{ M}$. The fit of the corresponding AMT measurement

(gray dashed line) provides a K_{D} value of $2.9 \times 10^{-4} \text{ M}$. Vertical lines represent the K_{D} value of AMO (yellow) and AMT (gray). **(c)** Analogous measurement to **(a)** of AMO (59 μM) with increasing concentration of G,C-only DNA in PBS buffer. Pure G,C-only DNA (4 mM) is depicted in pink. **(d)** A fit (red) of the absorbance at 340 nm versus the concentration of G,C-only DNA $[\text{DNA}]_{0, \text{GC}}$ from **(c)** yields $K_{\text{D}} = 6.9 \times 10^{-4} \text{ M}$ (yellow vertical line). The measurement on AMT shown here provides a K_{D} value of $4.7 \times 10^{-4} \text{ M}$

Fig. 1). Based on this rate constant and the fluorescence quantum yield, a fluorescence lifetime $\tau_{\text{fl}}^{\text{SB}} = \frac{\phi_{\text{fl}}}{k_{\text{r}}^{\text{SB}}}$ of 3.08 ns is predicted. By time-correlated single-photon counting (TCSPC), a value ($\tau_{\text{fl}}^{\text{TCSPC}} = 2.99$ ns) very close to this prediction is measured (see SI, Fig. S1).

3.2 Intercalation affinity

As outlined in the Introduction, intercalation is a requirement for photoaddition to DNA and thus is crucial for the photoreactive potential of AMO. To arrive at the respective dissociation constant K_{D} , first, the DNA concentrations were determined spectroscopically via Beer's law. The molar absorption coefficients per base pair at a wavelength of 300 nm, $\epsilon_{300\text{nm}}$, were computed for both synthetic DNA sequences (A,T-only DNA and G,C-only DNA)

based on the nearest-neighbor model [43]. The obtained values are $\epsilon_{300\text{nm}} = 260.8 \text{ M}^{-1} \text{ cm}^{-1}$ for A,T-only DNA and $\epsilon_{300\text{nm}} = 612.3 \text{ M}^{-1} \text{ cm}^{-1}$ for G,C-only DNA.

The results of the UV/Vis titration experiments on AMO with A,T-only DNA and G,C-only DNA are presented in Fig. 2. At low DNA concentrations (violet spectra), as expected, the spectra strongly resemble the one of AMO in water. At higher DNA concentrations (green spectra) and thus a large proportion of intercalated AMO, the absorption signal is lower. The dissociation constant K_{D} can be determined from the dependence of the absorption at 340 nm on the total DNA concentration $[\text{DNA}]_0$. The analysis employs the law of mass action and Beer's law (see Sect. 2). The derived K_{D} values are $8.9 \times 10^{-5} \text{ M}$ for AMO in A,T-only DNA and $6.9 \times 10^{-4} \text{ M}$ for AMO in G,C-only DNA. The dissociation constants K_{D} for AMT have previously been found

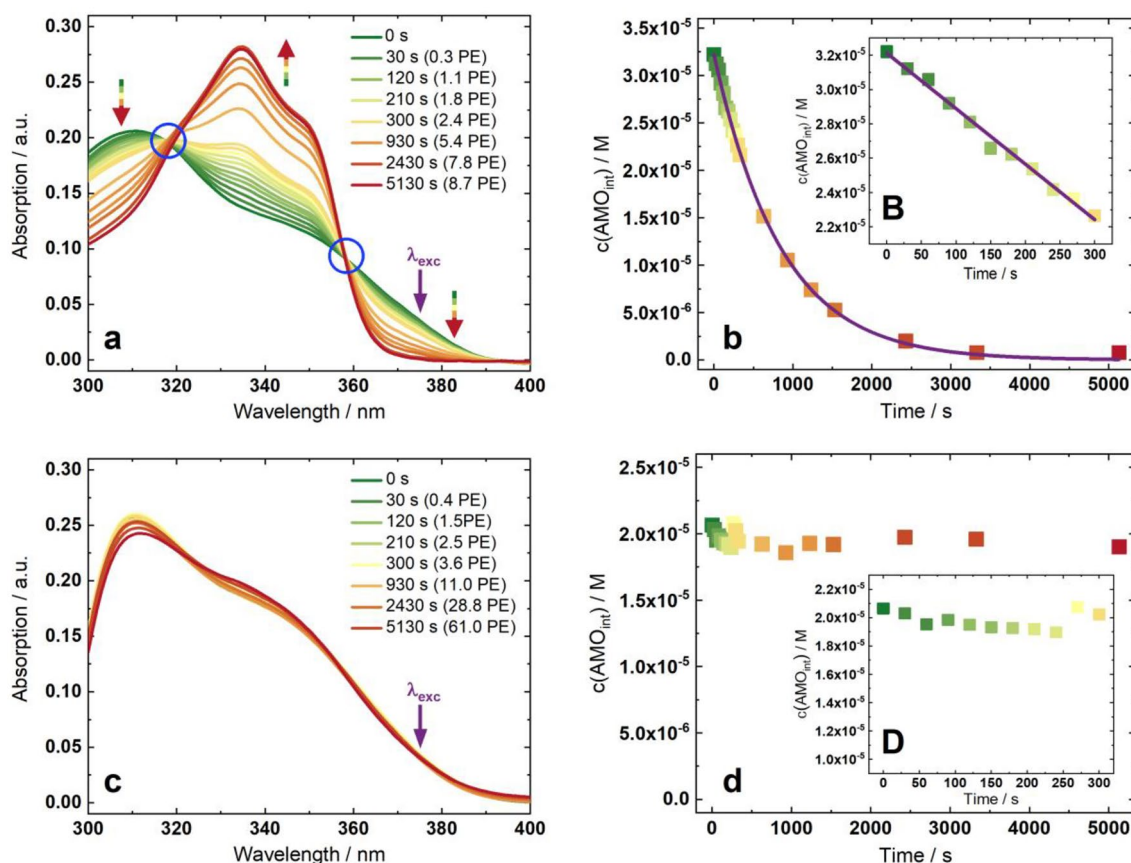


Fig. 3 Photoreactivity of AMO intercalated into A,T-only and G,C-only DNA traced by UV/Vis absorption. Exposure intervals are expressed in seconds as well as in photon equivalents (PE). Blue circles highlight isobestic points and colored arrows illustrate the decrease or increase of absorption with exposure time. Absorption contributions of DNA and free AMO were subtracted. (a) Spectra of AMO (35 μM) and A,T-only DNA (1 mM) in PBS buffer after depicted exposure times (green to red; $\lambda_{\text{exc}} = 375$ nm, $P = 3.75$ mW,

$V = 3$ mL, $d = 1$ cm). (b) Absorption at excitation wavelength (375 nm) versus the exposure time in seconds. A fit (violet line) affords a reaction quantum yield Φ_{R} of 0.11. (B) Linear region extracted from (b) with exposure intervals up to 300 s is shown. (c) Measurement on AMO (35 μM) intercalated into G,C-only DNA (1 mM) in PBS buffer. (d) Absorption at 375 nm versus the total exposure time from (c) and in (D) for exposure intervals up to 300 s were not fitted

to be 4.4×10^{-4} M (in A,T-only DNA) and 1.8×10^{-4} M (in G,C-only DNA) [30]. As experimental K_D values may vary with DNA manufacturers and annealing protocols, the measurements on AMT were repeated with DNA sample batches identical to the ones used for the AMO experiments. In these experiments, the magnitude of previous values for AMT could be reproduced with 2.9×10^{-4} M in A,T-only DNA, and 4.7×10^{-4} M in G,C-only DNA. The dissociation constant K_D for AMO in G,C-only DNA is in a similar range as those for AMT in G,C-only and in A,T-only DNA. However, the dissociation constant K_D for AMO in A,T-only DNA is smaller by approximately an order of magnitude. Thus, it may be stated with some confidence that AMO has a greater affinity for A,T-only DNA, whereas AMT has similar ones to both DNA types.

3.3 Photoreactivity

Depending on the DNA sequence, illumination of intercalated AMO with UV-A light leads to changes in the absorption spectrum (Fig. 3). Therefore, the photoreactivity of AMO with respect to DNA was probed by monitoring changes in the UV-A absorption upon illumination after defined time periods in seconds or photon equivalents (PE; see Sect. 2). At the applied concentrations of AMO and the respective DNA sequence, the amount of intercalated AMO is 0.92 for A,T-only DNA and 0.59 for G,C-only DNA. The contributions of free AMO to the absorption spectra was corrected for, and the spectra at $t=0$ in Fig. 2 are thus the ones of the intercalate. In order to monitor the photoreaction of AMO in DNA, an excitation wavelength of 375 nm was picked to avoid excitation of the DNA. For the exposure of AMO intercalated into A,T-only DNA (Fig. 3a), two isosbestic points are located at 318 nm and 358 nm. In between them, the absorption increases with increasing exposure time and PE. Below 315 nm and above 358 nm, the absorption decreases. The last spectrum (8.7 PE) shows the spectral signatures of the photoproduct. It features a maximum at ~ 340 nm with a shoulder around 350 nm. These characteristics indicate the formation of a furan side adduct [44]. Neither the pyrone monoadduct nor the crosslink absorb light in the UV-A range [11, 45]. Thus, the detection of these adducts by UV/Vis absorption spectroscopy is challenging. The spectroscopic pattern observed for the photoaddition of AMO to A,T-only DNA resembles qualitatively and quantitatively the one of AMT [31]. For other 4-methyl substituted psoralens, the predominance of the furan monoadduct was demonstrated chromatographically [45]. Therefore, it can reasonably be inferred that the furan monoadduct also prevails for AMO.

The approach used to determine the reaction quantum yield (see Sect. 2) rests on the assumption that the photoproduct does not absorb at the excitation wavelength.

Inspection of Fig. 3b shows that this is justified. At the excitation wavelength of 375 nm, the absorption decreases to essentially zero with increasing illumination time. The experimentally observed reduction of the reactant concentration $[AMO]_{int}$ with illumination time is well described by a fit employing Eq. (3). This fit yields a reaction quantum yield Φ_R of 0.11 (Fig. 3b). An analysis based on the early time behavior results in the same value (Fig. 3b). This value is close to the one of AMT_{int} ($\Phi_R=0.12$) [31], which could be reproduced in the present study ($\Phi_R=0.12$). For AMO intercalated into G,C-only DNA, only weak absorption changes with increasing illumination time are observed (Fig. 3c). As the signal at the excitation wavelength does not drop to zero or a constant value, a determination of the reaction quantum yield was not attempted.

3.4 Time-resolved spectroscopy

Femtosecond (fsTA; 100 fs–3 ns) and nanosecond (nsTA; 12 ns–70 μ s) transient absorption techniques were employed to temporally monitor spectral changes in the UV/Vis range in response to photoexcitation of AMO. The combined results of both techniques are presented in Fig. 4.

Right after excitation with fs-laser pulses at 330 nm, two excited state absorption (ESA) bands become apparent with maxima at 390 nm and 740 nm, as well as a shoulder at 680 nm. In addition, a very weak negative contribution around 500 nm is found, which can be assigned to stimulated emission (SE) of AMO. This assignment is supported by a comparison with the steady-state fluorescence spectrum (see Fig. 4). As SE gives a negative contribution to the difference absorption, the fluorescence spectrum was flipped horizontally. By shifting and scaling, it could be favorably overlaid with the short wavelength part of the TA spectrum. The small discrepancy at longer wavelengths is due to compensation by ESA. No evidence of ground state bleaching (GSB) is found throughout the entire time-frame and for all wavelengths. Except for slight shifts and changes in the band shapes, all described signatures remain for about 1 ns, until a significantly altered spectrum with absorption bands around 360 nm, 500 nm, and 650 nm emerges. This indicates the population of the triplet state T_1 of AMO, which can be further traced by nsTA. Immediately after excitation and transition to the triplet state, two difference absorption bands around 360 nm as well as between 450 and 700 nm are discernible.

A global multi-exponential fit [46] was conducted for both data sets to assess the kinetics of photoexcited AMO in water. The corresponding decay-associated difference spectra (DADS) are plotted in Fig. 5. The fsTA data were fitted satisfactorily with three time constants: $\tau_1=1$ ps, $\tau_2=46$ ps, and $\tau_3=2.99$ ns. In the fitting procedure, the value of the time constant τ_3 was not varied. The value ($\tau_{fl}^{TCSPC}=2.99$ ns)

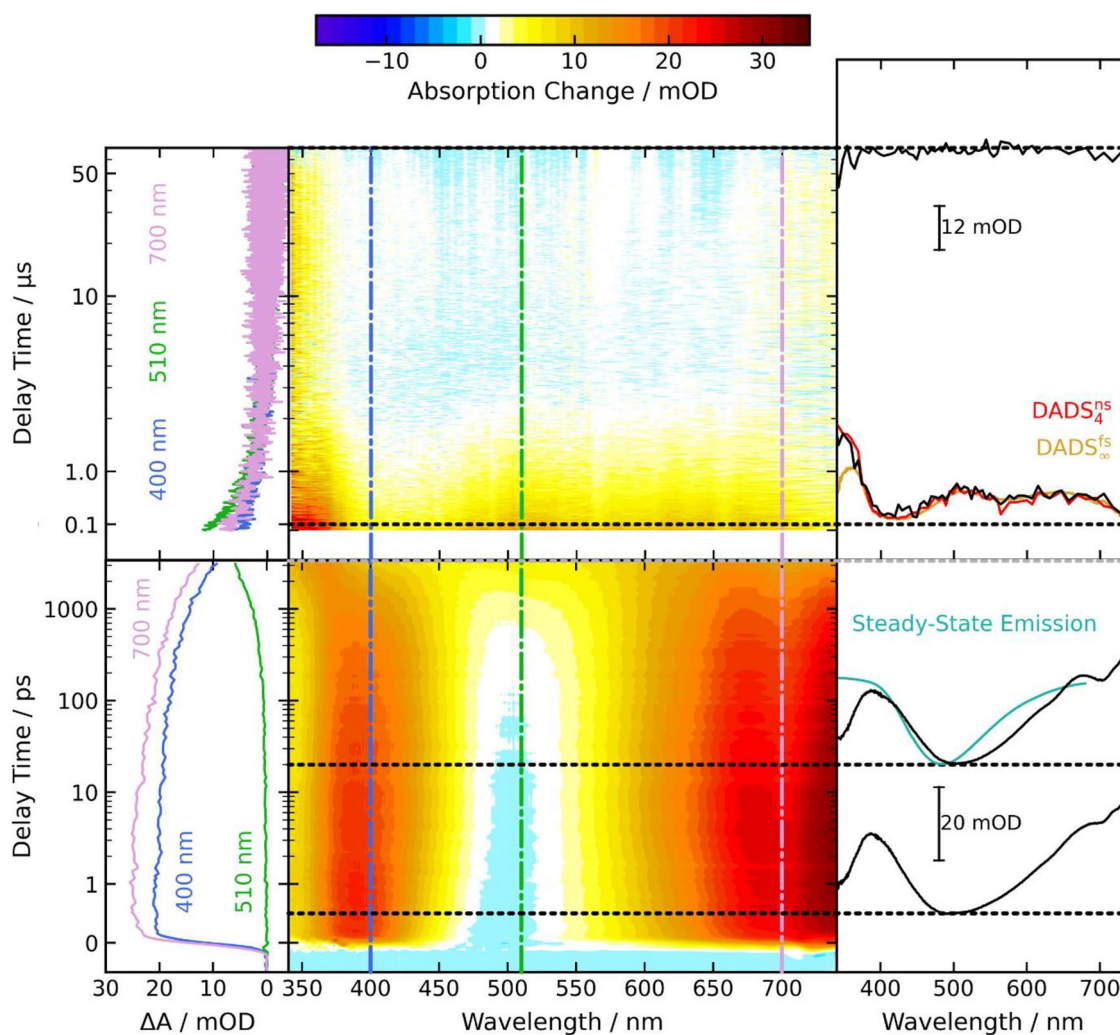


Fig. 4 Time-resolved spectroscopy on AMO in aerated water. In the fsTA experiment (lower panel), the excitation was tuned to 330 nm and the AMO concentration amounted to 0.3 mM. For the nsTA experiment (upper panel), the respective values were 355 nm and 0.18 mM. In the contour plot (center), the difference absorption signal is color-coded. Vertical lines in the contour plot indicate spectral positions for the time traces plotted on the left. Horizontal

lines denote certain delay times for the difference spectra plotted on the right. To highlight the contribution of the stimulated emission, a flipped steady-state emission spectrum of AMO (turquoise) is overlaid with the transient spectrum at 10 ps. The last decay-associated difference spectrum (DADS) from the fsTA experiment ($\text{DADS}_{\infty}^{\text{fs}}$ in yellow) is compared to the transient spectrum in the nsTA experiment after 0.1 μs and $\text{DADS}_4^{\text{ns}}$ (red)

from the TCSPC experiment was used. The $\text{DADS}_1^{\text{fs}}$ exhibits a sigmoidal feature around 400 nm and a negative contribution centered around 620 nm. In terms of absolute values, the amplitudes are small compared to the ones of $\text{DADS}_3^{\text{fs}}$ and $\text{DADS}_{\infty}^{\text{fs}}$. This pattern and the fact that the time constant τ_1 falls in the right range [47] suggest that dielectric relaxation of water causes the observed spectral changes. For the $\text{DADS}_2^{\text{fs}}$, two small positive bands are found at 375 nm and 680 nm. Between 500 and 550 nm, the signal is close to zero. Interestingly, the time constant τ_2 is not found in the closely related psoralen AMT [29]. An assignment of the time constant τ_2 is provided in the Discussion. The $\text{DADS}_3^{\text{fs}}$

features two pronounced positive bands around 400 nm and 680 nm. These positive bands indicate a decay of the ESA signal. Moreover, a negative contribution around 510 nm is recorded. This negative contribution is partially due to the decay of the SE and partially due to the rise of the triplet absorption. The DADS for “infinite” delay time ($\text{DADS}_{\infty}^{\text{fs}}$) in the fsTA experiment is compared with the DADS resulting from the decay monitored in the nsTA experiment ($\text{DADS}_4^{\text{ns}}$). The resemblance of these spectra underscores that no process is missing due to the temporal gap between 3 and 12 ns. These DADS are positive over the entire spectral range with a global maximum around 360 nm and two local maxima around 510 nm and 650 nm. The spectral pattern features

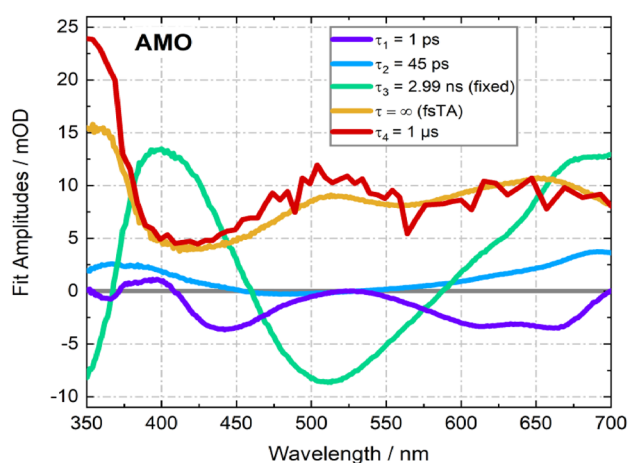


Fig. 5 Decay-associated difference spectra (DADS) obtained from the fsTA and nsTA experiments of AMO in aerated water

similarities to the triplet state of AMT [31]. The difference absorption decays to zero over the entire covered spectral range, with a lifetime τ_4 of 1 μs (aerated solution). When operating with oxygen-saturated water (~ 1 atm) instead of air, the lifetime is reduced to 0.2 μs . Deoxygenation by nitrogen purging prolongs the lifetime to 2.9 μs (see SI, Fig. S2). These experiments yield an oxygen-quenching rate constant of $k_q^{\text{O}_2} = 2.8 \times 10^9 \text{ M}^{-1} \text{ s}^{-1}$. The value is close to the one for AMT ($k_q^{\text{O}_2} = 3.3 \times 10^9 \text{ M}^{-1} \text{ s}^{-1}$ [31]). The mechanism of oxygen quenching has not been further investigated. However,

it is known that psoralen-type compounds are also capable of generating singlet oxygen involving triplet energy transfer according to type II photosensitization mechanism [48]. Potentially, this process can lead to photooxidative damage at the site of action. Self-quenching observed for AMT was not studied for AMO. For similar concentrations in aerated water, essentially identical lifetimes for AMT [31] and AMO were determined.

From the fsTA signatures of AMO in the presence of G,C-only DNA, the contribution of free psoralen was subtracted (see Sect. 2). Thus, the time-resolved spectra in Fig. 6 display only the signatures of the intercalated AMO. Immediately after excitation, the contour plot shows two positive difference absorption bands at 400 nm and 700 nm as well as a dip at 480 nm due to SE. These two ESA bands and the SE signature represent the S_1 state of photoexcited AMO. In comparison to AMO in the absence of DNA, the S_1 lifetime is strongly reduced to the picosecond range. An additional species is formed during the decay of these ESA bands, which, in turn, decays within several tens of picoseconds. The time trace at 510 nm illustrates the formation and decay of this species (see Fig. 6). After about 200 ps, the difference absorption has decayed to essentially zero. Thus, no nsTA measurement is needed. Based on the findings from steady-state illumination experiments and the previous studies on AMT with G,C-only DNA [29, 30], this spectro-temporal behavior is ascribed to a PET. Here, the base guanine donates an electron to the photoexcited AMO

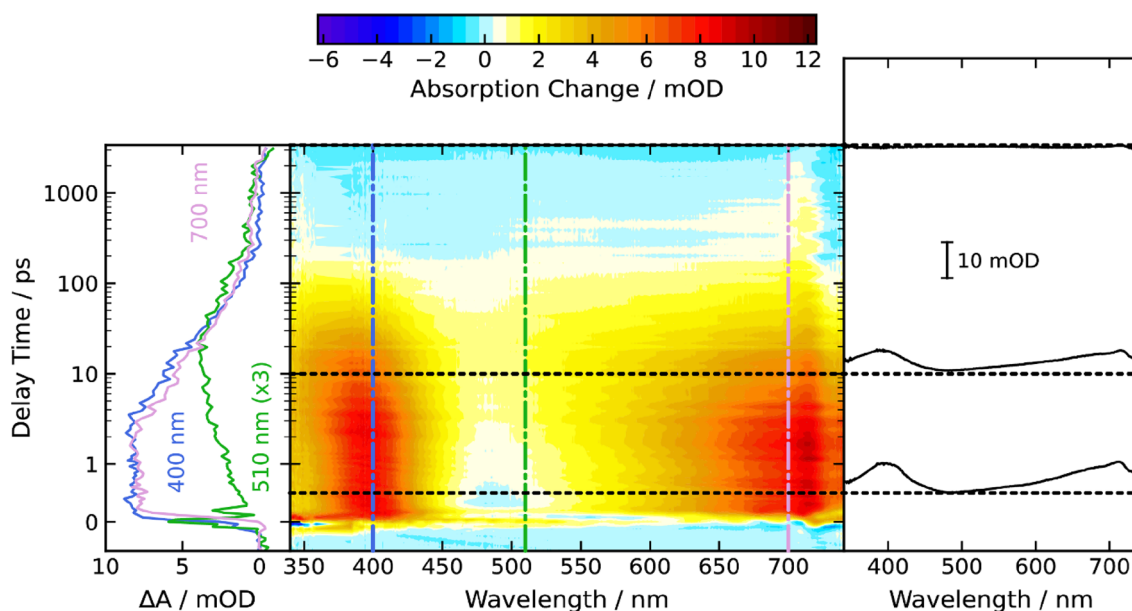


Fig. 6 Femtosecond transient absorption on AMO (0.3 mM) intercalated into G,C-only DNA (2.5 mM) in aqueous PBS buffer after excitation at 330 nm, corrected for the contributions of free AMO. Vertical dashed lines indicate the spectral position of the time traces on

the left, where the time trace at 510 nm was multiplied by a factor of three. Horizontal dashed lines in the contour plot indicate the temporal position of the transient spectra on the right

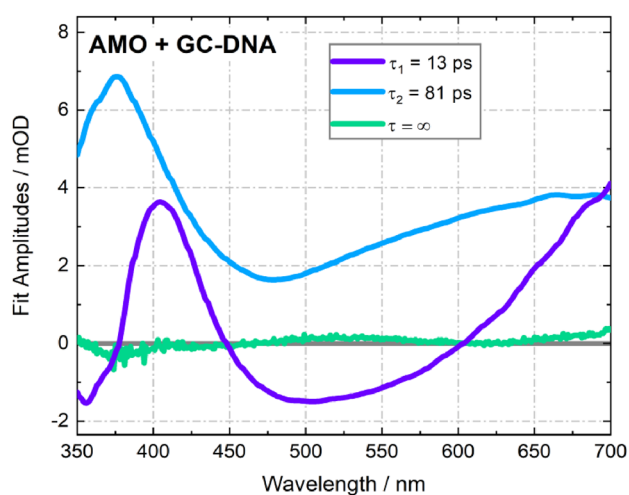


Fig. 7 DADS for the fsTA experiment on AMO with G,C-only DNA in aqueous PBS buffer

to form a radical pair according to type I photosensitization mechanism [49, 50].

A multi-exponential global fit of the data set yields time constants of $\tau_1 = 13$ ps and $\tau_2 = 81$ ps. The corresponding DADS are shown in Fig. 7. The DADS₁^{fs} features weak negative bands at 350 nm and 500 nm as well as positive ones at 400 nm and ~700 nm. The dip in the DADS₁^{fs} is due to SE decay and ESA rise of the intermediate. The DADS₂^{fs} is essentially the difference spectrum of the intermediate. It is positive throughout the covered spectral range and features bands at 375 nm and 680 nm. It strongly resembles the respective signature for AMT intercalated into G,C-only DNA [30]. This signature was assigned to be a radical pair consisting of a guanine cation radical and a psoralen anion radical [29, 30]. The remaining small signals in the offset spectrum (DADS_∞^{fs}) are presumably due to imperfections of the subtraction procedure.

The fsTA experiment on AMO intercalated into A,T-only DNA was performed and evaluated analogously to that with G,C-only DNA. In addition, the time window of fsTA was combined with the one from nsTA. Both experiments display a noisier difference absorption signal, as the intercalate consisting of AMO and A,T-only DNA absorbs less strongly than free AMO. At first glance, AMO in an A,T-rich environment (Fig. 8) seems to behave similarly to AMO in water, particularly in the femtosecond experiment. Immediately after excitation, two strong ESA bands around 390 nm and 740 nm are observable. In the DNA environment, no pronounced shoulder around 680 nm is apparent. The characteristic spectral signatures of the S₁ state are present for about 1 ns. Subsequently, a noticeably different spectrum is obtained with absorption bands around 370 nm and 510 nm. This signature is attributed to the formation of the triplet

state of AMO in presence of A,T-only DNA. Compared to AMO in the absence of DNA, the maximum around 510 nm is more distinct. The difference absorption signatures remain until the end of the accessible time window of the fsTA setup (~3.3 ns) and do not indicate any quenching caused by PET. This is consistent with our expectations, as there are no guanine bases in this DNA sequence and adenine cannot donate an electron due to thermodynamics [51].

In comparison to the fsTA experiment, the nsTA measurement exhibits a lower signal-to-noise ratio. Compared to the nsTA measurement of AMO in the absence of DNA, a longer temporal range of 40 ns to 330 μs was covered here. Immediately after excitation, positive difference absorption is evident throughout the covered spectral range. The transient spectrum after 2 μs coincides well with the offset spectrum of the fsTA experiment. Therefore, it can be assumed that no signatures of free AMO remain in this time domain. The signature attributed to the triplet state of AMO intercalated into A,T-only DNA decays within ~20 μs. Starting at about 100 μs, an increase in positive difference absorption is recorded around 350 nm. The last measured transient spectrum of the nsTA experiment was compared with a steady-state difference spectrum. This difference absorption spectrum was obtained from the steady-state illumination experiment in Fig. 3a. The observation that these spectra are similar in shape indicates that the photoproduct is formed within several 100 μs.

The fitted time constants with corresponding DADS related to the fsTA and nsTA measurements are compiled in Fig. 9. One time constant, $\tau_1 = 1090$ ps, proved to be sufficient to describe the fsTA measurement. The related DADS₁^{fs} shows positive difference bands around 410 nm and above 600 nm. Negative signal contributions are observed between 450 and 600 nm, reaching a global minimum around 500 nm. With reference to the fsTA experiment of AMO in absence of DNA, this time constant is attributed to the decay of the S₁ state. In comparison, a reduction of the S₁ lifetime of about 65% is found in the A,T-environment. The DADS for “infinite” delay time (DADS_∞^{fs}) shows positive difference absorption over the entire spectral range. Two maxima of equal magnitude are found at 375 nm and 510 nm. Based on the spectro-temporal features, this signature is ascribed to the triplet state of excited AMO intercalated into A,T-only DNA.

Due to the low signal-to-noise ratio of the nsTA experiment, a global analysis including the complete spectral range failed to describe the signal rise on the 100 μs time scale. Thus, the spectral range for fitting was first restricted to 315–402 nm. A global analysis relying on this range afforded time constants of $\tau_2 = 10$ μs and $\tau_3 = 600$ μs. Note that the value of τ_3 is larger than the longest delay time and thus subject to a large uncertainty. With the time constant τ_3

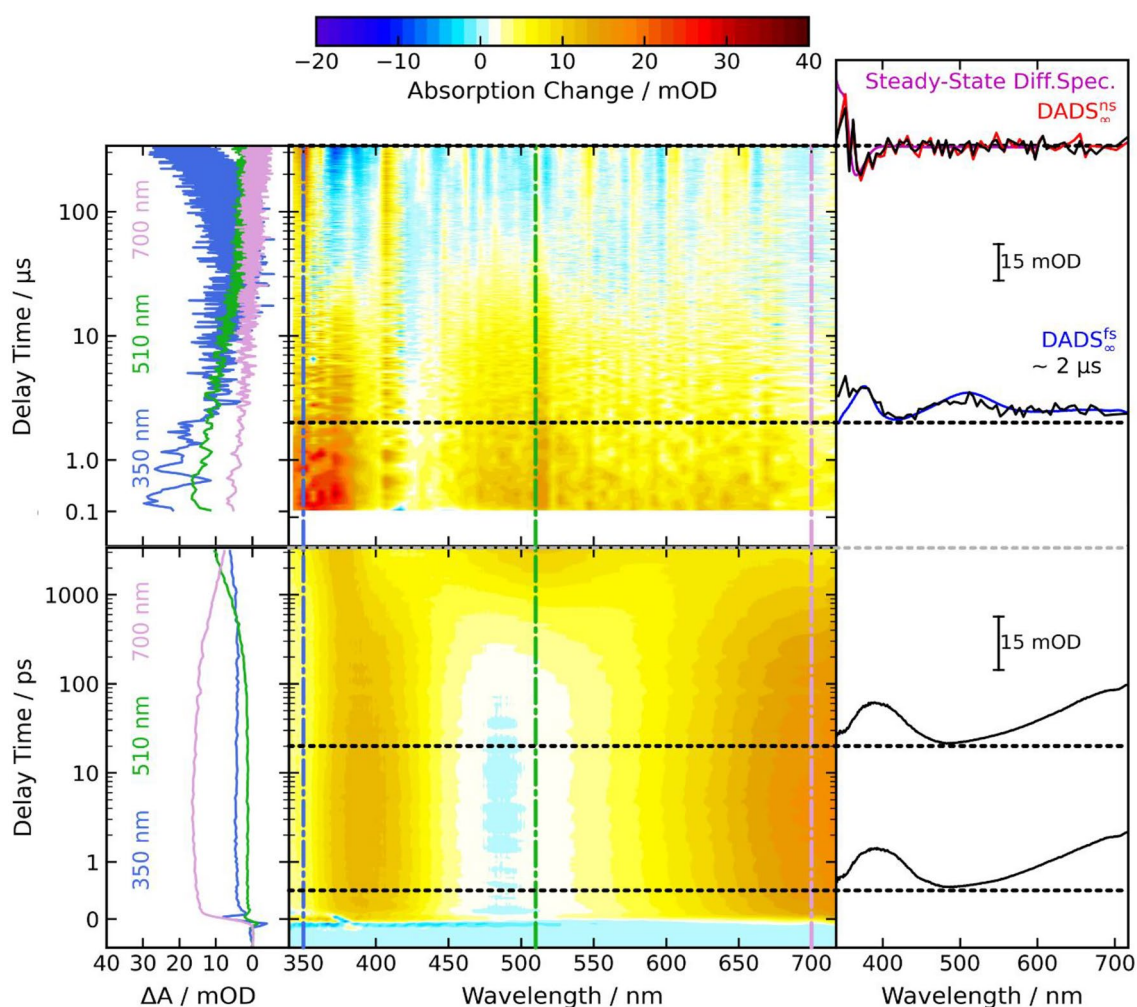


Fig. 8 Time-resolved spectroscopy on AMO intercalated into A,T-only DNA in aerated, aqueous PBS buffer. In the fsTA experiment (lower panel), the excitation was tuned to 330 nm, the AMO concentration amounted to 0.3 mM and the A,T-only DNA to 2.5 mM. For the nsTA experiment (upper panel), the respective values were 350 nm, 0.12 mM (AMO) and 0.4 mM (A,T-only DNA). The fsTA measurement was corrected for the contributions of free AMO. In the contour plot (center), the difference absorption signal is color-coded. Vertical lines in the contour plot indicate spectral positions for the

time traces plotted on the left. Horizontal lines denote delay times for the difference spectra plotted on the right. The last decay-associated difference spectrum (DADS) from the fsTA experiment, $DADS_{\infty}^{fs}$ (blue) is compared to the transient spectrum in the smoothed nsTA experiment (black) after 2 μ s. The “late” transient spectrum of the nsTA experiment is superimposed with the nsTA offset spectrum ($DADS_{\infty}^{ns}$ in red) and the scaled steady-state signature (purple; calculated from difference of absorption at 0 s and 5130 s from Fig. 3a)

fixed to 600 μ s and a variable constant τ_2 , the complete range was fitted. This slightly changed the constant τ_2 to 14 μ s. The DADS resulting from this procedure are shown in Fig. 9. The $DADS_2^{ns}$ is similar to the fsTA offset spectrum $DADS_{\infty}^{fs}$. Minor differences are found in the height and shift of the maximum at 375 nm. This finding can be ascribed to the emergence of a species after the formation of the triplet state of AMO, which has a comparable spectral signature. The time constant τ_2 of 14 μ s falls within a comparable range to the one determined for AMT in A,T-only DNA (6 μ s [31]). This time constant was assigned to the formation of a biradical between AMT and thymine [31]. The $DADS_3^{ns}$ exhibits

a weak negative absorption band between 350 and 360 nm, whereas a positive absorption band is seen around 380 nm. At wavelengths longer than 425 nm, fluctuating positive as well as negative contributions are observed. This might be due to a low signal-to-noise ratio of the measurement. The results of AMO in presence of A,T-only DNA display a longer time constant for the formation of a photoproduct ($\tau_3 = 600 \mu$ s) compared to the previous study on AMT in A,T-only DNA (49 μ s [31]). Lastly, $DADS_{\infty}^{ns}$ is presented in Fig. 9, which mainly shows a strong negative signal contribution around 380 nm. At shorter wavelengths, the difference absorption signal increases and appears to peak at

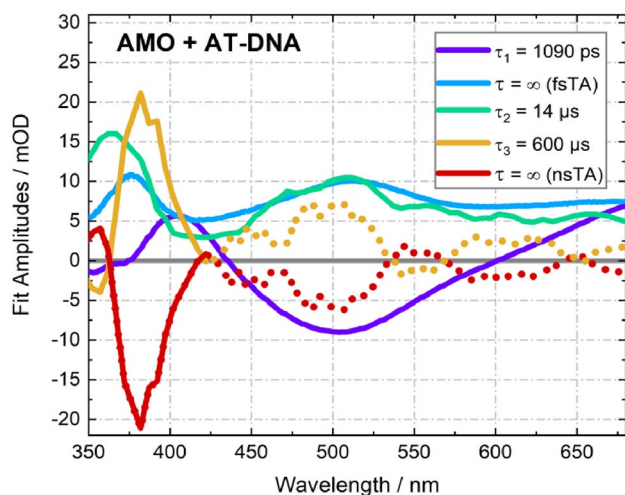


Fig. 9 DADS derived from fsTA and nsTA experiments on AMO intercalated into A,T-only DNA in aerated, aqueous buffer. In purple and blue, the DADS are shown, which are related to the fsTA measurement. The green, yellow and red DADS from the nsTA experiment were smoothed along the spectral axis. Dotted lines indicate fluctuations due to the low signal-to-noise ratio (see text)

350 nm. At wavelengths longer than 425 nm, the signal, which fluctuates around zero, exhibits no characteristic features. A comparison with the steady-state difference spectrum supports an assignment to the final photoproduct.

4 Discussion

Our previous spectroscopic studies on psoralens relied on synthetic derivatives such as our model system AMT [29–31] as well as naturally occurring psoralens, which are utilized in PUVA therapy [52]. In this study, we dealt for the first time with a psoralen derivative applied in the process of pathogen reduction in blood products, exploiting the same mechanism of action as PUVA. This derivative, namely AMO, shows a close structural similarity to AMT.

In line with our expectations, the photophysical properties of AMO strongly resemble those of AMT. In particular, AMO and AMT seem to exhibit the same features, with respect to the shape and position of the absorption bands. Minor differences between the two psoralen derivatives are found after exciting the samples and recording the fluorescence spectra. The fluorescence spectrum of AMO shows a maximum at 474 nm and thus is bathochromically shifted by ~20 nm compared to AMT. In addition, AMO exhibits a longer fluorescence lifetime ($\tau_{\text{fl}}^{\text{TCSPC}} = 3.08$ ns) and a higher fluorescence quantum yield ($\Phi_{\text{fl}} = 0.083$) compared to AMT. Moreover, an additional time constant of 45 ps is found in the fsTA experiment of AMO in absence of DNA. This additional time constant may be attributed to the cationic

tail of AMO. In psoralens (8-methoxy psoralen (8-MOP) and psoralen (PSO)) without this tail or one with a shorter carbon chain (AMT), this time constant is not detected. We speculate that the tail undergoes chain diffusion and thereby brings the ammonium group close to the chromophore. This, in turn, could slightly alter the transient spectrum. The respective time constant τ_2 of 45 ps is in the range observed for chain diffusion for this length [53].

More pronounced differences between AMO and AMT were seen in the intercalation experiments, whereas AMT [30] and other investigated psoralens [30, 52] displayed similar affinities (i.e., dissociation constants K_{D}) with respect to A,T-only and G,C-only DNA, the K_{D} value of AMO in A,T-only DNA is approximately one order of magnitude smaller than the one in G,C-only DNA. An order of magnitude in K_{D} translates in a difference of only few $\frac{\text{kJ}}{\text{mol}}$ for the respective Gibbs free energies ΔG^0 . Such a small difference is not amenable to a simple interpretation. Regardless of the interpretation, the difference in K_{D} values could be beneficial in terms of the PUVA process, since the photobinding proceeds with thymine bases. Provided that this prevails in “mixed” DNA containing A,T- and G,C-base pairs, it would “guide” AMO to preferentially intercalate in sites with photoreactive potential. In this context it is worth noting that pathogens whose DNA exhibits a low G,C-content (e.g., *P. falciparum* with ~25% [54] and *Staphylococcus* species with 30–35% [14, 55]) are inactivated to high levels by the AMO/UV-A light technology.

Concerning the photophysics of AMO in presence of G,C-only DNA, weak photoreactivity is observed in steady-state exposure experiments, akin to AMT [30]. fsTA measurements indicate that the photoexcited AMO intercalated into G,C-only DNA is quenched within tens of picoseconds, in line with the weak photoreactivity. This finding is attributed to a PET as mentioned in Sect. 3. Charge separation (CS) forming a radical pair $\text{G}^{\bullet+} \cdots \text{AMO}^{\bullet-}$ and charge recombination (CR) re-forming the starting material seems to proceed slightly slower than for AMT in G,C-only DNA ($\tau_{\text{CS}} = 13$ ps and $\tau_{\text{CR}} = 81$ ps compared to $\tau_{\text{CS}} = 4$ ps and $\tau_{\text{CR}} = 30$ ps [30]). In order to test whether the PET behavior of AMO follows the Marcus theory, the dependence of the PET rate constants ($k_{\text{CS/CR}}$) on the Gibbs free energies ($\Delta G_{\text{CS/CR}}^0$) were plotted (Fig. 10). For this purpose, the time constants for the formation and decay of the radical pair determined from the fsTA experiment were transformed into rate constants. The Gibbs free energies for CS and CR for the oxidation of guanine and reduction of AMO were calculated by means of Eqs. (8) and (9) reported in Fröbel et al. [30]. Assuming that, except for the 0–0 excitation energy E_{00} , all parameters of AMT may be applicable to AMO, and using $E_{00} = 3.15$ eV for AMO (see Sect. 3), Gibbs free energies

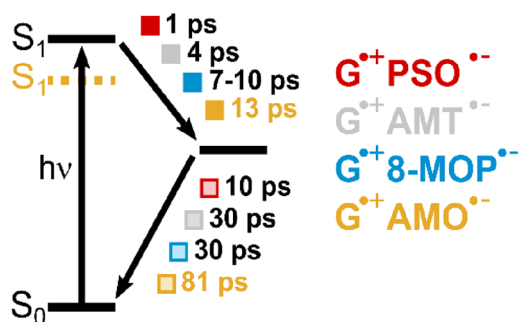
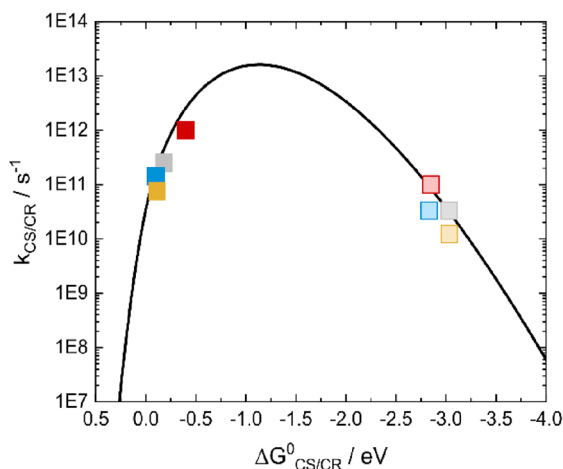


Fig. 10 Dependence of PET rate constants ($k_{CS/CR}$) on the driving force ($\Delta G_{CS/CR}^0$) of the previously investigated psoralens psoralen (PSO, red), AMT (grey), and 8-methoxy psoralen (8-MOP, blue) [30] as well as AMO (yellow) in G,C-only DNA. On the left, a kinetic scheme summarizing the time constants for charge separation (CS)

of $\Delta G_{CS}^0 = -0.11$ eV and $\Delta G_{CR}^0 = -3.03$ eV were calculated. The respective Gibbs free energies ΔG^0 and rate constants are compared with values of other psoralens in Fig. 10. The diagram shows that the PET kinetics of AMO are in line with the experimental values of other psoralens. Furthermore, it matches predictions by the Marcus-Levich-Jortner theory [56]. Despite the severe simplification of our estimates, the computed PET energies and the measured CS and CR rate constants coincide with the fit curve. Thus, AMO follows the Marcus theory like PSO, AMT and 8-MOP, which was previously published by Fröbel et al. (cf. Fig. 10). With adenine as a PET partner, a Gibbs free energy ΔG_{CS}^0 of 0.36 eV is computed (for the respective redox potentials see [51]). This process being endergonic is in line with the absence of PET here.

This analysis of the PET process shows that AMO, although acting as a type I photosensitizer here, does not cause irreversible lesions of G,C-only DNA. The radicals formed by photoexcitation recombine rapidly and thereby suppress subsequent irreversible processes.

In contrast to G,C-only DNA, the formation of a photoproduct is observed in an A,T-environment with a reaction quantum yield of $\Phi_R = 0.11$. Our previous study on AMT intercalated into A,T-only DNA yielded a comparable reaction quantum yield of $\Phi_R = 0.12$ [31]. Time-resolved measurements with femto- and nanosecond resolution confirm the photoreactivity of AMO intercalated into A,T-only DNA. Regarding the spectro-temporal signatures, the mechanism of the photoproduct formation is similar to AMT involving the local triplet state of AMO.



and charge recombination (CR) is provided. On the right, the determined PET data (filled squares for charge separation, hollow squares for charge recombination) are compared with a fit curve obtained by Lewis et al. [56] according to the Marcus-Levich-Jortner theory (black line) adapted by Fröbel et al. [30]

This local triplet is populated during the S_1 decay, which occurs within ~ 1 ns. The local triplet state decays to form a triplet biradical, which links the psoralen moiety and the thymine base by a C–C single bond. The process is somewhat slower in AMO ($\tau_2 = 14$ μs) compared to AMT ($\tau_2 = 6$ μs [31]). The final step leading from the biradical to the $C_4=C_5$ furan monoadduct (see Sect. 1) also seems to be slower for AMO when compared to AMT. We estimate a time constant of several 100 μs for AMO, whereas for AMT a photoproduct is formed within 49 μs . Yet, the reaction quantum yields Φ_R are essentially identical for both psoralens. This implies that for AMO intercalated into A,T-only DNA not only reactive processes but also processes re-forming the starting material, i.e., intercalated AMO in its electronic ground state, are slower. The fact that these microsecond processes are observed in aerated solution suggests that oxygen quenching is of minor relevance here. Such a “shielding” of intercalated chromophores from oxygen has been reported before [57].

5 Conclusions

In this study, the photophysics of the psoralen AMO employed in the INTERCEPT[®] Blood System was explored spectroscopically. A comparison with the closely related derivative AMT, which we have extensively characterized in previous studies, shows that AMO behaves similarly in the absence of DNA. In the presence of synthetic DNA bearing either adenine–thymine (A,T-only DNA) or guanine–cytosine bases (G,C-only DNA), UV/

Vis titration experiments were performed elucidating a higher intercalation affinity of AMO into A,T-only DNA compared to G,C-only DNA. Subsequent steady-state exposure experiments indicate AMO's photoreactivity as being comparable to that of AMT in A,T-only DNA and a weak photoreactivity in G,C-only DNA. Time-resolved measurements with femto- and nanosecond resolution are in agreement with these findings. They show signatures for photobinding to A,T-only DNA via the local triplet state of AMO and a biradical. On the other hand, a PET is observed in G,C-only DNA consistent with the Marcus theory. Photoaddition and PET were also observed in AMT but have shorter time constants. Both psoralens exhibit similar photophysics and -chemistry, thereby they seem to be potent candidates for pharmaceutical applications. However, the difference in intercalation affinity could be a crucial advantage of AMO as it favors the inhibition of DNA replication.

Supplementary Information The online version contains supplementary material available at <https://doi.org/10.1007/s43630-024-00545-2>.

Acknowledgements This work was founded by the Deutsche Forschungsgemeinschaft, grant number GI 349/6-2 as well as grant 396890929/GRK 2482, "ModISC". Michelle P. Rademacher is grateful for a scholarship of the Jürgen Manchot Foundation. Part of the data in this paper was presented at the 31st International Conference on Photochemistry in Sapporo, Japan on July 23–28, 2023 and at the 20th Congress of the European Society for Photobiology in Lyon, France on August 27–31, 2023.

Funding Open Access funding enabled and organized by Projekt DEAL.

Data availability Data will be made available on request.

Declarations

Conflict of interest On behalf of all the authors, the corresponding author states that there is no conflict of interest. Peter W. Bringmann is an employee of Cerus Corporation, a manufacturer of PRT.

Open Access This article is licensed under a Creative Commons Attribution 4.0 International License, which permits use, sharing, adaptation, distribution and reproduction in any medium or format, as long as you give appropriate credit to the original author(s) and the source, provide a link to the Creative Commons licence, and indicate if changes were made. The images or other third party material in this article are included in the article's Creative Commons licence, unless indicated otherwise in a credit line to the material. If material is not included in the article's Creative Commons licence and your intended use is not permitted by statutory regulation or exceeds the permitted use, you will need to obtain permission directly from the copyright holder. To view a copy of this licence, visit <http://creativecommons.org/licenses/by/4.0/>.

References

- Murray, R. D. H., Méndez, J., & Brown, S. A. (1982). *The natural coumarins: Occurrence, chemistry, and biochemistry*. Wiley.
- Fitzpatrick, T. B., & Pathak, M. A. (1959). Part IV: Basic considerations of the psoralens: Historical aspects of methoxsalen and other furocoumarins. *Journal of Investigative Dermatology*, 32(2), 229–231. <https://doi.org/10.1038/jid.1959.40>
- Pathak, M. A., & Fitzpatrick, T. B. (1992). The evolution of photochemotherapy with psoralens and UVA (PUVA): 2000 BC to 1992 AD. *Journal of Photochemistry Photobiology B: Biology*, 14(1–2), 3–22. [https://doi.org/10.1016/1011-1344\(92\)85080-E](https://doi.org/10.1016/1011-1344(92)85080-E)
- Kitamura, N., Kohtani, S., & Nakagaki, R. (2005). Molecular aspects of furocoumarin reactions: Photophysics, photochemistry, photobiology, and structural analysis. *Journal of Photochemistry Photobiology C: Photochemistry Reviews*, 6(2–3), 168–185. <https://doi.org/10.1016/j.jphotochemrev.2005.08.002>
- Menter, A., Korman, N. J., Elmets, C. A., Feldman, S. R., Gelfand, J. M., Gordon, K. B., Gottlieb, A., Koo, J. Y. M., Lebwohl, M., Leonardi, C. L., Lim, H. W., Van Voorhees, A. S., Beutner, K. R., Ryan, C., & Bhushan, R. (2011). Guidelines of care for the management of psoriasis and psoriatic arthritis: Section 6. Guidelines of care for the treatment of psoriasis and psoriatic arthritis: case-based presentations and evidence-based conclusions. *Journal of the American Academy of Dermatology* 65(1), 137–174. <https://doi.org/10.1016/j.jaad.2010.11.055>.
- Sidbury, R., Davis, D. M., Cohen, D. E., Cordoro, K. M., Berger, T. G., Bergman, J. N., Chamlin, S. L., Cooper, K. D., Feldman, S. R., Hanifin, J. M., Krol, A., Margolis, D. J., Paller, A. S., Schwarzenberger, K., Silvermann, R. A., Simpson, E. L., Tom, W. L., Williams, H. C., Elmets, C. A., Block, J., Harrod, C. G., Begolka, W. S., & Eichenfeld, L. F. (2014). Guidelines of care for the management of atopic dermatitis: Section 3. Management and treatment with phototherapy and systemic agents. *Journal of the American Academy of Dermatology* 71(2), 327–349. <https://doi.org/10.1016/j.jaad.2014.03.030>.
- Taieb, A., Alomar, A., Böhm, M., Dell'Anna, M. L., De Pase, A., Eleftheriadou, V., Ezzedine, K., Gauthier, Y., Gawkrödger, D. J., Jouary, T., Leone, G., Moretti, S., Nieuweboer-Krobotova, L., Olsson, M. J., Parsad, D., Passeron, T., Tanew, A., van der Veen, W., van Geel, N., ... Picardo, M. (2013). Guidelines for the management of vitiligo: The European Dermatology Forum consensus. *British Journal of Dermatology*, 168(1), 5–19. <https://doi.org/10.1111/j.1365-2133.2012.11197.x>
- Olsen, E. A., Hodak, E., Anderson, T., Carter, J. B., Henderson, M., Cooper, K., & Lim, H. W. (2016). Guidelines for phototherapy of mycosis fungoides and Sézary syndrome: A consensus statement of the United States Cutaneous Lymphoma Consortium. *Journal of the American Academy of Dermatology*, 74(1), 27–58. <https://doi.org/10.1016/j.jaad.2015.09.033>
- Thompson, J. F., & Hearst, J. E. (1983). Structure of *E. coli* 16S RNA elucidated by psoralen crosslinking. *Cell* 32(4), 1355–1365. [https://doi.org/10.1016/0092-8674\(83\)90316-1](https://doi.org/10.1016/0092-8674(83)90316-1).
- Rinke, J., Appel, B., Digweed, M., & Lüthmann, R. (1985). Localization of a base-paired interaction between small nuclear RNAs U4 and U6 in intact U4/U6 ribonucleoprotein particles by psoralen cross-linking. *Journal of Molecular Biology*, 185(4), 721–731. [https://doi.org/10.1016/0022-2836\(85\)90057-9](https://doi.org/10.1016/0022-2836(85)90057-9)
- Cimino, G. D., Gamper, H. B., Isaacs, S. T., & Hearst, J. E. (1985). Psoralens as photoactive probes of nucleic acid structure and function: Organic chemistry, photochemistry, and biochemistry. *Annual Review of Biochemistry*, 54(1), 1151–1193. <https://doi.org/10.1146/annurev.bi.54.070185.005443>
- Lu, Z., Zhang, Q. C., Lee, B., Flynn, R. A., Smith, M. A., Robinson, J. T., Davidovich, C., Gooding, A. R., Goodrich, K. J., Mattick, J. S., Mesirov, J. P., Cech, T. R., & Chang, H. Y. (2016). RNA duplex map in living cells reveals higher-order transcriptome structure. *Cell*, 165(5), 1267–1279. <https://doi.org/10.1016/j.cell.2016.04.028>

13. Zhang, M., Li, K., Bai, J., Velema, W. A., Yu, C., van Damme, R., Lee, W. H., Corpuz, M. L., Chen, J.-F., & Lu, Z. (2021). Optimized photochemistry enables efficient analysis of dynamic RNA structuromes and interactomes in genetic and infectious diseases. *Nature Communications*, *12*(1), 2344. <https://doi.org/10.1038/s41467-021-22552-y>
14. Irsch, J., & Lin, L. (2011). Pathogen inactivation of platelet and plasma blood components for transfusion using the INTERCEPT Blood System. *Transfusion Medicine and Hemotherapy*, *38*(1), 19–31. <https://doi.org/10.1159/000323937>
15. Bagri, A., de Assis, R. R., Tsai, C. T., Simmons, G., Mei, Z. W., Von Goetz, M., Gatmaitan, M., Stone, M., Di Germanio, C., Martinelli, R., Darst, O., Rioveros, J., Robinson, P. V., Ward, D., Ziman, A., Seftel, D., Khan, S., Busch, M. P., Felgner, P. L., & Corash, L. M. (2022). Antibody profiles in COVID-19 convalescent plasma prepared with amotosalen/UVA pathogen reduction treatment. *Transfusion*, *62*(3), 570–583. <https://doi.org/10.1111/trf.16819>
16. Green, A. B., Chiaraviglio, L., Truelson, K. A., Zulauf, K. E., Cui, M., Zhang, Z., Ware, M. P., Flegel, W. A., Haspel, R. L., Yu, E. W., & Kirby, J. E. (2023). RND pump-mediated efflux of Amotosalen, a compound used in pathogen inactivation technology to enhance safety of blood transfusion products, may compromise its gram-negative anti-bacterial activity. *mSphere*, *8*(2), e0067322. <https://doi.org/10.1128/msphere.00673-22>
17. Horowitz, B., Lazo, A., Grossberg, H., Page, G., Lippin, A., & Swan, G. (1998). Virus inactivation by solvent/detergent treatment and the manufacture of SD-plasma. *Vox Sanguinis*, *74*(S1), 203–206. <https://doi.org/10.1111/j.1423-0410.1998.tb05473.x>
18. Wagner, S. J. (2002). Virus inactivation in blood components by photoactive phenothiazine dyes. *Transfusion Medicine Reviews*, *16*(1), 61–66. <https://doi.org/10.1053/tmrv.2002.29405>
19. Kaiser-Guignard, J., Canellini, G., Lion, N., Abonnenc, M., Osselaer, J.-C., & Tissot, J.-D. (2014). The clinical and biological impact of new pathogen inactivation technologies on platelet concentrates. *Blood Reviews*, *28*(6), 235–241. <https://doi.org/10.1016/j.blre.2014.07.005>
20. Goodrich, R. P., Edrich, R. A., Li, J., & Seghatchian, J. (2006). The Mirasol™ PRT system for pathogen reduction of platelets and plasma: An overview of current status and future trends. *Transfusion and Apheresis Science*, *35*(1), 5–17. <https://doi.org/10.1016/j.transci.2006.01.007>
21. Seltsam, A., & Müller, T. H. (2011). UVC irradiation for pathogen reduction of platelet concentrates and plasma. *Transfusion Medicine and Hemotherapy*, *38*(1), 43–54. <https://doi.org/10.1159/000323845>
22. Escolar, G., Diaz-Ricart, M., & McCullough, J. (2022). Impact of different pathogen reduction technologies on the biochemistry, function, and clinical effectiveness of platelet concentrates: An updated view during a pandemic. *Transfusion*, *62*(1), 227–246. <https://doi.org/10.1111/trf.16747>
23. Lanteri, M. C., Santa-Maria, F., Laughhunn, A., Girard, Y. A., Picard-Maureau, M., Payrat, J. M., Irsch, J., Stassinopoulos, A., & Bringmann, P. (2020). Inactivation of a broad spectrum of viruses and parasites by photochemical treatment of plasma and platelets using amotosalen and ultraviolet A light. *Transfusion*, *60*(6), 1319–1331. <https://doi.org/10.1111/trf.15807>
24. Lin, L., Dikeman, R., Molini, B., Lukehart, S. A., Lane, R., Dupuis, K., Metzler, P., & Corash, L. (2004). Photochemical treatment of platelet concentrates with amotosalen and long-wavelength ultraviolet light inactivates a broad spectrum of pathogenic bacteria. *Transfusion*, *44*(10), 1496–1504. <https://doi.org/10.1111/j.1537-2995.2004.04125.x>
25. Castro, G., Merkel, P. A., Giclas, H. E., Gibula, A., Andersen, G. E., Corash, L. M., Lin, J. S., Green, J., Knight, V., & Stassinopoulos, A. (2018). Amotosalen/UVA treatment inactivates T cells more effectively than the recommended gamma dose for prevention of transfusion-associated graft-versus-host disease. *Transfusion*, *58*(6), 1506–1515. <https://doi.org/10.1111/trf.14589>
26. Singh, Y., Sawyer, L. S., Pinkoski, L. S., Dupuis, K. W., Hsu, J. C., Lin, L., & Corash, L. (2006). Photochemical treatment of plasma with amotosalen and long-wavelength ultraviolet light inactivates pathogens while retaining coagulation function. *Transfusion*, *46*(7), 1168–1177. <https://doi.org/10.1111/j.1537-2995.2006.00867.x>
27. Hearst, J. E., Isaacs, S. T., Kanne, D., Rapoport, H., & Straub, K. (1984). The reaction of the psoralens with deoxyribonucleic acid. *Quarterly Reviews of Biophysics*, *17*(1), 1–44. <https://doi.org/10.1017/S0033583500005242>
28. Bethea, D., Fullmer, B., Syed, S., Seltzer, G., Tiano, J., Rischko, C., Gillespie, L., Brown, D., & Gasparro, F. P. (1999). Psoralen photobiology and photochemotherapy: 50 years of science and medicine. *Journal of Dermatological Science*, *19*(2), 78–88. [https://doi.org/10.1016/S0923-1811\(98\)00064-4](https://doi.org/10.1016/S0923-1811(98)00064-4)
29. Fröbel, S., Reiffers, A., Torres Ziegenbein, C., & Gilch, P. (2015). DNA intercalated psoralen undergoes efficient photoinduced electron transfer. *Journal of Physical Chemistry Letters*, *6*(7), 1260–1264. <https://doi.org/10.1021/acs.jpcclett.5b00307>
30. Fröbel, S., Levi, L., Ulamec, S. M., & Gilch, P. (2016). Photoinduced electron transfer between psoralens and DNA: Influence of DNA sequence and substitution. *ChemPhysChem*, *17*(9), 1377–1386. <https://doi.org/10.1002/cphc.201500889>
31. Diekmann, J., Gontcharov, J., Fröbel, S., Torres Ziegenbein, C., Zinth, W., & Gilch, P. (2019). The photoaddition of a psoralen to DNA proceeds via the triplet state. *Journal of the American Chemical Society*, *141*(34), 13643–13653. <https://doi.org/10.1021/jacs.9b06521>
32. Berg, J. M., Tymoczko, J. L., Gatto, G. J., Jr., & Stryer, L. (2015). *Biochemistry*. New York: W. H. Freeman and Company.
33. Pal, H., Nad, S., & Kumbhakar, M. (2003). Photophysical properties of coumarin-120: Unusual behavior in nonpolar solvents. *Journal of Chemical Physics*, *119*(1), 443–452. <https://doi.org/10.1063/1.1578057>
34. El-Gogary, T. M., & El-Gendy, E. M. (2003). Noncovalent attachment of psoralen derivatives with DNA: Hartree-Fock and density functional studies on the probes. *Spectrochimica Acta Part A: Molecular Biomolecular Spectroscopy*, *59*(11), 2635–2644. [https://doi.org/10.1016/S1386-1425\(03\)00038-6](https://doi.org/10.1016/S1386-1425(03)00038-6)
35. Laimgruber, S., Schachenmayr, H., Schmidt, B., Zinth, W., & Gilch, P. (2006). A femtosecond stimulated Raman spectrograph for the near ultraviolet. *Applied Physics B*, *85*, 557–564. <https://doi.org/10.1007/s00340-006-2386-8>
36. Bertling, J., Thom, K. A., Geenen, S., Jeuken, H., Presser, L., Müller, T. J. J., & Gilch, P. (2021). Synthesis and photophysics of water-soluble psoralens with red-shifted absorption. *Photochemistry and Photobiology*, *97*(6), 1534–1547. <https://doi.org/10.1111/php.13480>
37. Nolden, O., Kremper, J., Haselbach, W., Morshedi, M., Guhl, J., Schmeinck, P., Marian, C. M., Ganter, C., & Gilch, P. (2023). Femtosecond spectroscopy and quantum chemistry of a linearly coordinated copper (I) carbene complex. *ChemPhotoChem*, *7*(4), e202200231. <https://doi.org/10.1002/cptc.202200231>
38. Lorenc, M., Ziolk, M., Naskrecki, R., Karolczak, J., Kubicki, J., & Maciejewski, A. (2002). Artifacts in femtosecond transient absorption spectroscopy. *Applied Physics B*, *74*, 19–27. <https://doi.org/10.1007/s003400100750>
39. Haselbach, W., Kaminski, J. M., Kloeters, L. N., Müller, T. J. J., Weingart, O., Marian, C. M., Gilch, P., & Nogueira de Faria, B. E. (2023). A thermally activated delayed fluorescence emitter investigated by time-resolved near-infrared spectroscopy. *Chemistry—A*

- European Journal 29(2), e202202809. <https://doi.org/10.1002/chem.202202809>.
40. Tatchen, J., & Marian, C. M. (2006). Vibronic absorption, fluorescence, and phosphorescence spectra of psoralen: A quantum chemical investigation. *Physical Chemistry Chemical Physics*, 8(18), 2133–2144. <https://doi.org/10.1039/B518436C>
 41. Parson, W. W., & Burda, C. (2022). Modern optical spectroscopy: From fundamentals to applications in chemistry, biochemistry and biophysics. Springer. <https://doi.org/10.1007/978-3-031-17222-9>
 42. Strickler, S. J., & Berg, R. A. (1962). Relationship between absorption intensity and fluorescence lifetime of molecules. *Journal of Chemical Physics*, 37(4), 814–822. <https://doi.org/10.1063/1.1733166>
 43. Tataurov, A. V., You, Y., & Owczarzy, R. (2008). Predicting ultraviolet spectrum of single stranded and double stranded deoxyribonucleic acids. *Biophysical Chemistry*, 133(1–3), 66–70. <https://doi.org/10.1016/j.bpc.2007.12.004>
 44. Oroskar, A., Olack, G., Peak, M. J., & Gasparro, F. P. (1994). 4'-Aminomethyl-4, 5', 8-trimethylpsoralen photochemistry: The effect of concentration and UVA fluence on photoadduct formation in poly(dA-dT) and calf thymus DNA. *Photochemistry and Photobiology*, 60(6), 567–573. <https://doi.org/10.1111/j.1751-1097.1994.tb05149.x>
 45. Kanne, D., Rapoport, H., & Hearst, J. E. (1984). 8-Methoxypsoralen-nucleic acid photoreaction. Effect of methyl substitution on pyrone vs. furan photoaddition. *Journal of Medicinal Chemistry* 27(4), 531–534. <https://doi.org/10.1021/jm00370a017>.
 46. Satzger, H., & Zinth, W. (2003). Visualization of transient absorption dynamics—towards a qualitative view of complex reaction kinetics. *Chemical Physics*, 295(3), 287–295. <https://doi.org/10.1016/j.chemphys.2003.08.012>
 47. Bagchi, B., & Jana, B. (2010). Solvation dynamics in dipolar liquids. *Chemical Society Reviews*, 39(6), 1936–1954. <https://doi.org/10.1039/B902048A>
 48. Parsons, B. J. (1980). Psoralen photochemistry. *Photochemistry and Photobiology*, 32(6), 813–821. <https://doi.org/10.1111/j.1751-1097.1980.tb04061.x>
 49. Baptista, M. S., Cadet, J., Di Mascio, P., Ghogare, A. A., Greer, A., Hamblin, M. R., Lorente, C., Nunez, S. C., Ribeiro, M. S., & Thomas, A. H. (2017). Type I and type II photosensitized oxidation reactions: Guidelines and mechanistic pathways. *Photochemistry and Photobiology*, 93(4), 912–919. <https://doi.org/10.1111/php.12716>
 50. Baptista, M. S., Cadet, J., Greer, A., & Thomas, A. H. (2021). Photosensitization reactions of biomolecules: Definition, targets and mechanisms. *Photochemistry and Photobiology*, 97(6), 1456–1483. <https://doi.org/10.1111/php.13470>
 51. Seidel, C. A. M., Schulz, A., & Sauer, M. H. M. (1996). Nucleobase-specific quenching of fluorescent dyes. I. Nucleobase one-electron redox potentials and their correlation with static and dynamic quenching efficiencies. *Journal of Physical Chemistry* 100(13), 5541–5553. <https://doi.org/10.1021/jp951507c>.
 52. Diekmann, J., Theves, I., Thom, K. A., & Gilch, P. (2020). Tracing the photoaddition of pharmaceutical psoralens to DNA. *Molecules*, 25(22), 5242. <https://doi.org/10.3390/molecules25225242>
 53. Fierz, B., Satzger, H., Root, C., Gilch, P., Zinth, W., & Kiefhaber, T. (2007). Loop formation in unfolded polypeptide chains on the picoseconds to microseconds time scale. *Proceedings of the National Academy of Sciences*, 104(7), 2163–2168. <https://doi.org/10.1073/pnas.0611087104>
 54. Grellier, P., Benach, J., Labaied, M., Charneau, S., Gil, H., Monsalve, G., Alfonso, R., Sawyer, L., Lin, L., & Steiert, M. (2008). Photochemical inactivation with amotosalen and long-wavelength ultraviolet light of Plasmodium and Babesia in platelet and plasma components. *Transfusion*, 48(8), 1676–1684. <https://doi.org/10.1111/j.1537-2995.2007.01762.x>
 55. Fadeyi, E. A., Wagner, S. J., Goldberg, C., Lu, T., Young, P., Bringmann, P. W., Meier, N. M., Namen, A. M., Benjamin, R. J., & Palavecino, E. (2021). Fatal sepsis associated with a storage container leak permitting platelet contamination with environmental bacteria after pathogen reduction. *Transfusion*, 61(2), 641–648. <https://doi.org/10.1111/trf.16210>
 56. Lewis, F. D., Kalgutkar, R. S., Wu, Y., Liu, X., Liu, J., Hayes, R. T., Miller, S. E., & Wasielewski, M. R. (2000). Driving force dependence of electron transfer dynamics in synthetic DNA hairpins. *Journal of the American Chemical Society*, 122(49), 12346–12351. <https://doi.org/10.1021/ja0028267>
 57. Berkoff, B., Hogan, M., Legrange, J., & Austin, R. (1986). Dependence of oxygen quenching of intercalated methylene blue triplet lifetime on DNA base-pair composition. *Biopolymers: Original Research on Biomolecules* 25(2), 307–316. <https://doi.org/10.1002/bip.360250211>